

We are IntechOpen, the world's leading publisher of Open Access books Built by scientists, for scientists

6,900

Open access books available

186,000

International authors and editors

200M

Downloads

Our authors are among the

154

Countries delivered to

TOP 1%

most cited scientists

12.2%

Contributors from top 500 universities



WEB OF SCIENCE™

Selection of our books indexed in the Book Citation Index
in Web of Science™ Core Collection (BKCI)

Interested in publishing with us?
Contact book.department@intechopen.com

Numbers displayed above are based on latest data collected.
For more information visit www.intechopen.com



Mass Transfer Related to Heterogeneous Combustion of Solid Carbon in the Forward Stagnation Region - Part 2 - Combustion Rate in Special Environments

Atsushi Makino
Japan Aerospace Exploration Agency
Japan

1. Introduction

Carbon combustion is a research subject, indispensable for practical utilization of coal combustion, ablative carbon heat-shields, and/or aerospace applications with carbon-carbon composites (C/C-composites). Because of this practical importance, extensive research has been conducted not only experimentally but also theoretically and/or numerically, and several reviews (Batchelder, et al., 1953; Gerstein & Coffin, 1956; Walker, et al., 1959; Clark, et al., 1962; Khitrin, 1962; Mulcahy & Smith, 1969; Maahs, 1971; Rosner, 1972; Essenhigh, 1976, 1981; Annamalai & Ryan, 1993; Annamalai, et al., 1994) describe the accomplishments in this field, as mentioned in Part 1. Nevertheless, because of the complexities involved, there still remain several problems that must be clarified to understand basic nature of carbon combustion.

In Part 1, after describing general characteristics of the carbon combustion, it was intended to represent it by use of some of the basic characteristics of the chemically reacting boundary layers (Chung, 1965; Law, 1978), under recognition that flow configurations are indispensable for proper evaluation of the heat and mass transfer, especially for the situation in which the gas-phase reaction can intimately affect overall combustion response through its coupling to the surface reactions. The flow configuration chosen was that of the stagnation-flow, which is a well-defined, one-dimensional flow, being characterized by a single parameter, called the stagnation velocity gradient, offering various advantages for mathematical analyses, experimental data acquisition, and/or physical interpretations.

Specifically, formulation of the governing equations was first presented in Part 1, based on theories on the chemically reacting boundary layer. Chemical reactions considered were the surface C-O₂ and C-CO₂ reactions and the gas-phase CO-O₂ reaction. Generalized species-enthalpy coupling functions were then derived without assuming any limit or near-limit behaviors, which not only enable us to minimize the extent of numerical efforts needed for generalized treatment, but also provide useful insight into the conserved scalars in the carbon combustion. After that, it was shown that straightforward derivation of the combustion response could be allowed in the limiting situations, such as those for the Frozen, Flame-detached, and Flame-attached modes.

Next, after presenting profiles of gas-phase temperature, measured over the burning carbon, a further analytical study was conducted about the ignition phenomenon, related to finite-rate kinetics in the gas phase, by use of the asymptotic expansion method to obtain a critical condition for the appearance of the CO-flame. Appropriateness of this criterion was further examined by comparing temperature distributions in the gas phase and/or surface temperatures at which the CO-flame could appear. After having constructed these theories, evaluations of kinetic parameters for the surface and gas-phase reactions were then conducted, in order for further comparisons with experimental results.

In this Part 2, it is intended to make use of the information obtained in Part 1, for exploring carbon combustion, further. First, in order to decouple the close coupling between surface and gas-phase reactions, an attempt is conducted to raise the velocity gradient as high as possible, in Section 2. It is also endeavored to obtain explicit combustion-rate expressions, even though they might be approximate, because they are anticipated to contribute much to the foundation of theoretical understanding of carbon combustion, offering mathematical simplifications, just like that in droplet combustion, and to the practical applications, such as designs of ablative carbon heat shields and/or structures with C/C-composites in oxidizing atmospheres.

After having examined appropriateness of the explicit expressions, carbon combustion in the high-temperature airflow is then examined in Section 3, relevant to the High-Temperature Air Combustion, which is anticipated to have various advantages, such as energy saving, utilization of low-calorific fuels, reduction of nitric oxide emission, etc. The carbon combustion in the high-temperature, humid airflow is also examined theoretically in Section 4, by extending formulations for the system with three surface reactions and two global gas-phase reactions. Existence of a new burning mode with suppressed H_2 ejection from the surface can be confirmed for the carbon combustion at high temperatures when the velocity gradient of the humid airflow is relatively low. Some other results relevant to the High-Temperature Air Combustion are further shown in Section 5.

Concluding remarks not only for Part 2 but also for Part 1 are made in Section 6, with references cited and nomenclature tables.

2. Combustion response in high stagnation flowfields

It has been recognized that phenomena of carbon combustion become complicated upon the appearance of CO-flame, as pointed out in Part 1. Then, another simpler combustion response, being anticipated to be observed by suppressing its appearance, by use of the high velocity gradients, would provide useful insight into the carbon combustion, as well as facilitate deeper understanding for it. In addition, under simplified situations, there is a possibility that we could find out an explicit combustion-rate expression that can further contribute much to the foundation of theoretical understanding of the carbon combustion, offering mathematical simplifications, just like that in droplet combustion. Various contributions to practical applications, such as designs of furnaces, combustors, ablative carbon heat-shields, and high-temperature structures with C/C-composites in oxidizing atmosphere, are also anticipated.

2.1 Experimental results for the combustion rate

Figure 1(a) shows the combustion rate (Makino, et al., 1998b) as a function of the surface temperature, with the velocity gradient taken as a parameter. The H_2O mass-fraction in

airflow is set to be 0.003. Data points are experimental and solid curves are results of combustion-rate expressions to be mentioned. When the velocity gradient is 200 s^{-1} , the same trend as those in Figs. 2 and 8 in Part 1 is observed. That is, with increasing surface temperature, the combustion rate first increases, then decreases abruptly, and again increases. In Fig. 1(a), the ignition surface-temperature predicted is also marked.

As the velocity gradient is increased up to 640 s^{-1} , the combustion rate becomes high, due to an enhanced oxidizer supply, but the trend is still the same. A further increase in the velocity gradient, however, changes the trend. When the velocity gradient is 1300 s^{-1} , which is even higher than that ever used in the previous experimental studies (Matsui, et al., 1975; 1983; 1986), the combustion rate first increases, then reaches a plateau, and again increases, as surface temperature increases. Since the ignition surface-temperature is as high as 1970 K , at which the combustion rate without CO-flame is nearly the same as that with CO-flame, no significant decrease occurs in the combustion rate. On the contrary, a careful observation suggests that there is a slight, discontinuous increase in the combustion rate just after the appearance of CO-flame.

Since the ignition surface-temperature strongly depends on the velocity gradient (Visser & Adomeit, 1984; Makino & Law, 1990), as explained in Section 4 in Part 1, the discontinuous change in the combustion rate, caused by the appearance of CO-flame, ceases to exist with

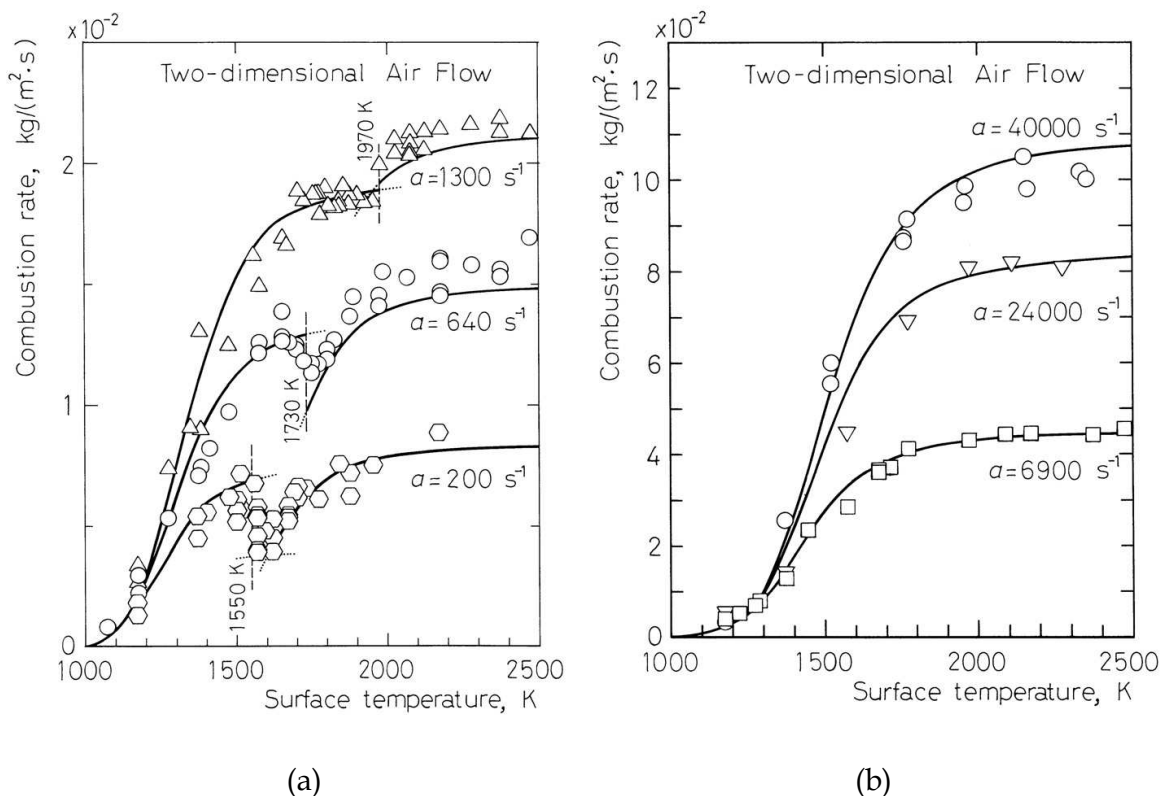


Fig. 1. Combustion rate as a function of the surface temperature, with the velocity gradient taken as a parameter (Makino, et al., 1998b), (a) when there appears CO-flame within the experimental conditions; (b) when the velocity gradient is at least one order of magnitude higher than that ever used in the previous studies. Oxidizer is air and its H_2O mass-fraction is 0.003. Data points are experimental with the test specimen of $1.25 \times 10^3 \text{ kg}/\text{m}^3$ in graphite density; curves are results of the explicit combustion-rate expressions.

increasing velocity gradient, as shown in Fig. 1(b). Here, use has been made of a graphite rod with a small diameter (down to 5 mm), as well as airflow with high velocity (up to 50 m/s). We see that the combustion rate increases monotonically with increasing surface temperature. Note that the velocity gradient used here is at least one order of magnitude higher than those in previous works.

As for the “negative temperature coefficient” of the combustion rate, examined in the literature (*cf.* Essenhigh, 1981), a further comment is required because it completely disappears at high velocity gradients. This experimental fact suggests that it has nothing to do with chemical events, related to the surface reactions, hitherto examined. Although it is described in the literature that some (Nagel and Strickland-Constable, 1962) attributed it to the sites of surface reactions and others (Yang and Steinberg, 1977) did it to the reaction depth, Figs. 1(a) and 1(b) certainly suggest that this phenomenon is closely related to the gas-phase reaction, which can even be blown off when the velocity gradients are high.

2.2 Approximate, explicit expressions for the combustion rate

In order to calculate the combustion rate, temperature profiles in the gas phase must be obtained by numerically solving the energy conservation equation for finite gas-phase reaction kinetics. However, if we note that carbon combustion proceeds with nearly frozen gas-phase chemistry until the establishment of the CO-flame (Makino, et al., 1994; Makino, et al., 1996) and that the combustion is expected to proceed under nearly infinite gas-phase kinetics once the CO-flame is established, analytically-obtained combustion rates (Makino, 1990; Makino, 1992), presented in Section 3 in Part 1, are still useful for practical utility.

However, it should also be noted that the combustion-rate expressions thus obtained are implicit, so that further numerical calculations are required by taking account of the relation, $\beta \equiv (-f_s)/(\xi')_s$, which is a function of the streamfunction f . Since this procedure is slightly complicated and cannot be used easily in practical situations, explicit expressions are anxiously required, in order to make these results more useful.

In order to elucidate the relation between the nondimensional combustion rate $(-f_s)$ and the transfer number β (Spalding, 1951), dependence of $(\xi')_s$ on the profile of the streamfunction f is first to be examined, by introducing a simplified profile of f as

$$f = \begin{cases} f_s & (0 \leq \eta \leq \eta^*) \\ b\eta + c & (\eta^* \leq \eta \leq \eta^{**}) \\ \eta + d & (\eta \geq \eta^{**}) \end{cases}, \quad (1)$$

as shown in Fig. 2(a), and then conducting an integration. Here, b , c , and d are constants, $f(\eta^*) = f_s$, and $f(\eta^{**}) = f_o$.

Recalling the definitions of β and $(\xi')_s$, and making use of a relation, $(-f_s) \ll 1$, as is the case for most solid combustion, we have the following approximate relation:

$$1 + \beta \approx \exp[K(-f_s)] \quad \text{or} \quad (-f_s) \approx \frac{\ln(1 + \beta)}{K}, \quad (2)$$

where

$$K = \eta^* + \sqrt{\frac{\pi}{2}} \left[\left\{ \exp\left(\frac{(b-1)f_o^2}{2b}\right) - 1 \right\} \operatorname{erfc}\left(\frac{f_o}{\sqrt{2}}\right) - \left(1 - \frac{1}{\sqrt{b}}\right) \operatorname{erf}\left(\frac{f_o}{\sqrt{2}}\right) \right] + \sqrt{\frac{\pi}{2}}. \quad (3)$$

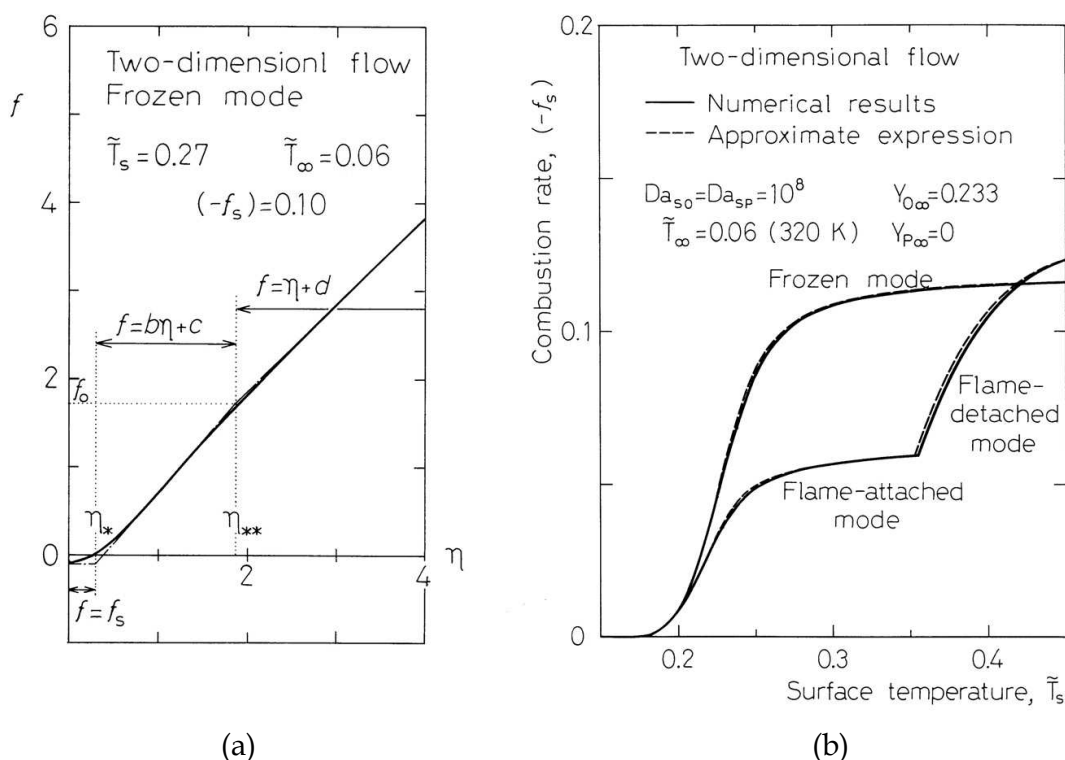


Fig. 2.(a) A profile of the streamfunction f for the two-dimensional stagnation flow, as a function of the boundary-layer variable η , when the surface temperature $T_s \approx 1450$ K, the ambient temperature $T_\infty \approx 320$ K, and the combustion rate $(-f_s) = 0.10$. The solid curve is the result obtained by a numerical calculation, and the dashed curve is the simplified profile used to find out the approximate expression (Makino, et al., 1998b). (b) Combustion rates for the three limiting modes in the stagnation airflow as a function of the surface temperature when the surface Damköhler number for the C-O₂ reaction, Da_{sO} , and that for the C-CO₂ reaction, Da_{sP} , are 10^8 . The solid curves are results of the implicit expressions and dashed curves are those of the explicit expressions.

Equation (2) shows that the combustion rate $(-f_s)$ can be expressed by the transfer number β in terms of the logarithmic term, $\ln(1+\beta)$. Note that the first and second terms in Eq. (3) are one order of magnitude smaller than the third term $(\pi/2)^{1/2}$.

In order to obtain the specific form of the transfer number β , a two term expansion of the exponential function is expected to be sufficient because $(-f_s) \ll 1$, so that use has been made of the following relation (Makino, 1992; Makino, et al., 1998b).

$$\frac{\beta}{1+\beta} = 1 - \exp[-K(-f_s)] \approx K(-f_s) \tag{4}$$

By virtue of this relation, Eqs. (44), (47), and (55) in Part 1 can yield the following approximate expressions for the transfer number.

Frozen mode:

$$\beta \approx \left(\frac{KA_{s,O}}{1+KA_{s,O}} \right) \left(\frac{\tilde{Y}_{O,\infty}}{\delta} \right) + \left(\frac{KA_{s,P}}{1+KA_{s,P}} \right) \left(\frac{\tilde{Y}_{P,\infty}}{\delta} \right) \tag{5}$$

Flame-detached mode:

$$\beta \approx \left(\frac{KA_{s,P}}{1+KA_{s,P}} \right) \left(\frac{\tilde{Y}_{O,\infty} + \tilde{Y}_{P,\infty}}{\delta} \right) \quad (6)$$

Flame-attached mode:

$$\beta \approx \left(\frac{KA_{s,O}}{1+2KA_{s,O}-KA_{s,P}} \right) \left(\frac{\tilde{Y}_{O,\infty}}{\delta} \right) + \left(\frac{KA_{s,P}}{1+2KA_{s,O}-KA_{s,P}} \right) \left(\frac{\tilde{Y}_{P,\infty}}{\delta} \right) \quad (7)$$

Although these are approximate, the transfer number can be expressed explicitly, in terms of the reduced surface Damköhler numbers, $A_{s,O}$ and $A_{s,P}$, and O_2 and CO_2 concentrations in the freestream.

In addition, we have

$$KA_{s,i} = k_{s,i} \frac{K}{\sqrt{2^j a (\mu_\infty/\rho_\infty)}} ; \quad k_{s,i} \equiv B_{s,i} \left(\frac{\tilde{T}_\infty}{\tilde{T}_s} \right) \exp \left(-\frac{\tilde{T}a_{s,i}}{\tilde{T}_s} \right) \quad (i = O, P), \quad (8)$$

where $k_{s,i}$ is the specific reaction rate constant for the surface reaction. Note that the factor, $K/[2^j a (\mu_\infty/\rho_\infty)]^{1/2}$, in Eq. (8) also appears in the combustion rate defined in Eq. (32) in Part 1, by use of the relation in Eq. (2), as

$$\dot{m} \approx \rho_\infty \frac{\sqrt{2^j a (\mu_\infty/\rho_\infty)}}{K} \ln(1+\beta). \quad (9)$$

2.3 Correction factor K and mass-transfer coefficient

In order to elucidate the physical meaning of the factor, $K/[2^j a (\mu_\infty/\rho_\infty)]^{1/2}$, let us consider a situation that $\beta \ll 1$, with the Frozen mode combustion taken as an example. Then, Eq. (9) leads to the following result:

$$\dot{m} \approx \frac{1}{\frac{1}{k_{s,O}} + \frac{1}{\sqrt{2^j a (\mu_\infty/\rho_\infty)}}} \rho_\infty \left(\frac{\tilde{Y}_{O,\infty}}{\delta} \right) + \frac{1}{\frac{1}{k_{s,P}} + \frac{1}{\sqrt{2^j a (\mu_\infty/\rho_\infty)}}} \rho_\infty \left(\frac{\tilde{Y}_{P,\infty}}{\delta} \right). \quad (10)$$

We see that this expression is similar to the well-known expression for the solid combustion rate,

$$\dot{m} = \frac{1}{\frac{1}{k_s} + \frac{1}{h_D}} (\rho Y_O)_\infty, \quad (11)$$

for the first-order kinetics (Fischbeck, 1933; Fischbeck, et al., 1934; Tu, et al., 1934; Frank-Kamenetskii, 1969). Here, h_D is the overall convective mass-transfer coefficient. It is seen that the factor, $[2^j a (\mu_\infty/\rho_\infty)]^{1/2}/K$, corresponds to the mass-transfer coefficient h_D , suggesting that the specific form of h_D is of use in determining a form of the correction factor K .

Furthermore, by evaluating mass fluxes at the surface and in the gas phase, with the elemental carbon, $(W_C/W_F)Y_{F+}(W_C/W_P)Y_P$, taken as the transferred substance, and by use of the coupling function in Eq. (33) in Part 1, we have

$$h_D = \left(\frac{\tilde{T}_R}{\tilde{T}_\infty} \right) (\xi')_s \sqrt{2^j a (\mu_\infty/\rho_\infty)}, \quad (12)$$

suggesting that the correction factor K depends on both $(\xi')_s$ and the representative temperature T_R in the boundary layer.

2.4 Approximate expression for the correction factor K

In obtaining an approximate expression for the factor K , it seems that we can use the accomplishment in the field of heat and mass transfer. The mass-transfer coefficient is given as (Katto, 1982; White, 1988).

Two-dimensional Stagnation Flow:

$$h_D = \left(\frac{\tilde{T}_R}{\tilde{T}_\infty} \right) \frac{0.570}{Sc^{0.6}} \sqrt{a (\mu_\infty/\rho_\infty)} \quad \text{from} \quad \frac{Nu_x}{\sqrt{Re_x}} = 0.570 Sc^{0.4}, \quad (13)$$

Axisymmetric Stagnation Flow:

$$h_D = \left(\frac{\tilde{T}_R}{\tilde{T}_\infty} \right) \frac{0.540}{Sc^{0.6}} \sqrt{2a (\mu_\infty/\rho_\infty)} \quad \text{from} \quad \frac{Nu_x}{\sqrt{Re_x}} = 0.763 Sc^{0.4}, \quad (14)$$

based on the analogy between heat and mass transfers, where

$$Nu_x = \frac{h_D x}{D_R}, \quad Re_x = \frac{\rho_R U x}{\mu_R}, \quad U = ax, \quad Sc = \frac{\mu/\rho}{D}. \quad (15)$$

However, this kind of expression is far from satisfactory because Eqs. (13) and (14) are originally obtained for heat-transfer problems without mass transfer. In addition, this relation is obtained under an assumption that there is no density change, even though there exist temperature and/or concentration distributions in the gas phase.

Because of the simultaneous existence of temperature and concentration distributions in the carbon combustion, we are required to obtain an approximate expression for the factor K in another way. In this attempt, $(\pi/2)^{1/2}$ in the factor K in Eq. (3) is kept as it is because it is $1/(\xi')_s$ for inviscid stagnation flow without mass ejection from the surface. The remaining part of the factor K is then determined by use of numerical results (Makino, 1990; Makino, et al., 1994; Makino, et al., 1996). In this determination, use has been made of a curve-fitting method, with (T_∞/T_s) taken as a variable, to have a simple function. It has turned out that we can fairly represent the combustion rate for the Frozen and/or Flame-attached modes in two-dimensional stagnation flow with

$$K = \left(\frac{\tilde{T}_\infty}{\tilde{T}_s} \right) \left(1 - \frac{\tilde{T}_\infty}{2\tilde{T}_s} \right) + \sqrt{\frac{\pi}{2}}, \quad (16)$$

within 3% error when the O_2 mass-fraction $Y_{O,\infty}$ is 0.233 (cf. Fig. 2(b); Makino, et al., 1998b); for $Y_{O,\infty}=0.533$, error is within 5%; for $Y_{O,\infty}=1$, error is within 8%. Examinations have been made in the range of the surface Damköhler numbers $Da_{s,O}$ and $Da_{s,P}$ from 10^6 to 10^{10} , that of the surface temperature T_s from 1077 K to 2424 K, and that of the freestream temperature T_∞ from 323 K to 1239 K. The Frozen and Flame-attached modes can fairly be correlated by the single Eq. (16) because the gas-phase temperature profiles are the same. Note that the combustion rate in high O_2 concentrations violates the assumption that $(-f_s) \ll 1$. Nonetheless, the expressions appear to provide a fair representation because these expressions vary as the natural logarithm of the transfer number.

For axisymmetric stagnation flow, it turns out that the combustion rate in the Frozen and/or Flame-attached modes can fairly be represented with

$$K = \sqrt{\frac{2}{3} \left(\frac{\tilde{T}_\infty}{\tilde{T}_s} \right) \left(1 - \frac{\tilde{T}_\infty}{2\tilde{T}_s} \right)} + \sqrt{\frac{\pi}{2}}, \quad (17)$$

within 3% error for $Y_{O,\infty}=0.233$ (Makino, et al., 1998b); within 5% error for $Y_{O,\infty}=0.7$. Difference in the forms between Eq. (16) and Eq. (17) can be attributed to the difference in the flow configuration.

For the combustion rate in the Flame-detached mode, not only the surface and freestream temperatures but also the oxidizer concentration must be taken into account. It has turned out that

$$K = \left(\frac{\tilde{T}_\infty}{\tilde{T}_s} \right) \left(1 - \frac{\tilde{T}_\infty}{2\tilde{T}_s} \right) - 0.05 (1 + 2\tilde{Y}_{O,\infty}) + \sqrt{\frac{\pi}{2}} \quad (18)$$

can fairly represent the combustion rate in two-dimensional stagnation flow, within 4% error when the O_2 mass-fraction $Y_{O,\infty}$ is 0.233 and 0.533, although the error becomes 6% near the transition state for the flame attaches. In an oxygen flow, the error is within 6% except for the transition state, while it increases up to 15% around the state.

For axisymmetric stagnation flow, the combustion rate in the Flame-detached mode can be represented with

$$K = \sqrt{\frac{2}{3} \left(\frac{\tilde{T}_\infty}{\tilde{T}_s} \right) \left(1 - \frac{\tilde{T}_\infty}{2\tilde{T}_s} \right)} - 0.05 (1 + 2\tilde{Y}_{O,\infty}) + \sqrt{\frac{\pi}{2}}. \quad (19)$$

The error is nearly the same as that for the two-dimension case.

2.5 Experimental comparisons at high velocity gradients

In order to verify the validity of the explicit combustion-rate expressions, comparisons have been made with their values and the experimental results (Makino, et al., 1998b). Kinetic parameters are those evaluated in Section 5 in Part 1. The values of thermophysical properties are those at $T_\infty=320$ K, which yields $\rho_\infty\mu_\infty=2.12 \times 10^{-5}$ kg²/(m⁴·s) and $\mu_\infty/\rho_\infty=1.78 \times 10^{-5}$ m²/s. Results for the explicit combustion-rate expressions are shown in Figs. 1(a) and 1(b) by solid curves. As shown in Fig. 1(a), up to the ignition surface-temperature, a reasonable prediction can be made by Eq. (2), with the transfer number β for the Frozen mode in Eq. (5) and the correction factor K in Eq. (16), for two-dimensional case.

When the surface temperature is higher than the ignition surface-temperature, Eq. (2) with β for the Flame-detached mode in Eq. (6) and K in Eq. (18) can fairly represent the experimental results, except for the temperatures near the ignition surface-temperature, especially, in airflow with low velocity-gradient, say, 200 s^{-1} . In this temperature range, we can use Eq. (2) with β for the Flame-attached mode in Eq. (7) and K in Eq. (16) although accuracy of this prediction is not so high, compared to the other cases. This is attributed to the fact that we cannot assume the gas-phase reaction rate infinitely fast because the combustion situation is that just after the establishment of CO-flame.

When the velocity gradient is high, as shown in Fig. 1(b), the expression in Eq. (2) with β for the Frozen mode in Eq. (5) and K in Eq. (16) fairly represents the experimental results, up to about 2500 K in the surface temperature.

3. High-temperature air combustion

Here, carbon combustion has been examined, relevant to the High-Temperature Air Combustion, characterized by use of hot air ($\sim 1280 \text{ K}$) and attracted as one of the new technology concepts for pursuing energy saving and/or utilization of low-calorific fuels. Although it has been confirmed to reduce NO_x emission through reduction of O_2 concentration in furnaces, without reducing combustion rate of gaseous and/or liquid fuels (Katsuki & Hasegawa, 1998; Tsuji, et al., 2003), its appropriateness for solid-fuel combustion has not been examined fully. Since solid fuels are commonly used as one of the important energy sources in industries, it is strongly required to examine its appropriateness from the fundamental viewpoint. Here, focus is put on examinations for the promoting and suppressing effects that the temperature and water vapor in the airflow have. From the practical point of view, the carbon combustion in airflow at high temperatures, especially, in high velocity gradients, is related to evaluation of ablative carbon heat-shield for atmospheric re-entry. As for that in airflow at high H_2O concentrations, it is related to evaluation of protection properties of rocket nozzles, made of carbonaceous materials, from erosive attacks of water vapor, contained in working fluid for propulsion, as well as the coal/char combustion in such environments with an appreciable amount of water vapor.

3.1 Combustion in relatively dry airflow

Figure 3(a) shows the combustion rate as a function of the surface temperature T_s , with the airflow temperature T_∞ taken as a parameter. The H_2O mass-fraction $Y_A=0.003$ in the airflow, considered to be dry, practically. The combustion rate in the high-temperature airflow ($T_\infty=1280 \text{ K}$), shown by a solid diamond, increases monotonically and reaches the diffusion-limited value with increasing T_s . Monotonic change in the combustion rate is attributed to the high velocity gradient ($a=3300 \text{ s}^{-1}$), which is too high for the CO-flame to be established (Makino, et al., 2003), so that the combustion here is considered to proceed solely with the surface C- O_2 reaction. Note that this velocity gradient has been chosen, so as to suppress the abrupt changes in the combustion rates, in order to clarify effects of the High-Temperature Air Combustion.

Results in the room-temperature airflow ($T_\infty=320 \text{ K}$) with the same mass flow rate ($a=820 \text{ s}^{-1}$) are also shown. The combustion rate first increases, then decreases abruptly, and again increases, with increasing T_s , as explained in the previous Section. The ignition surface-temperature observed is about 1800 K, in accordance with the abrupt decrease in the

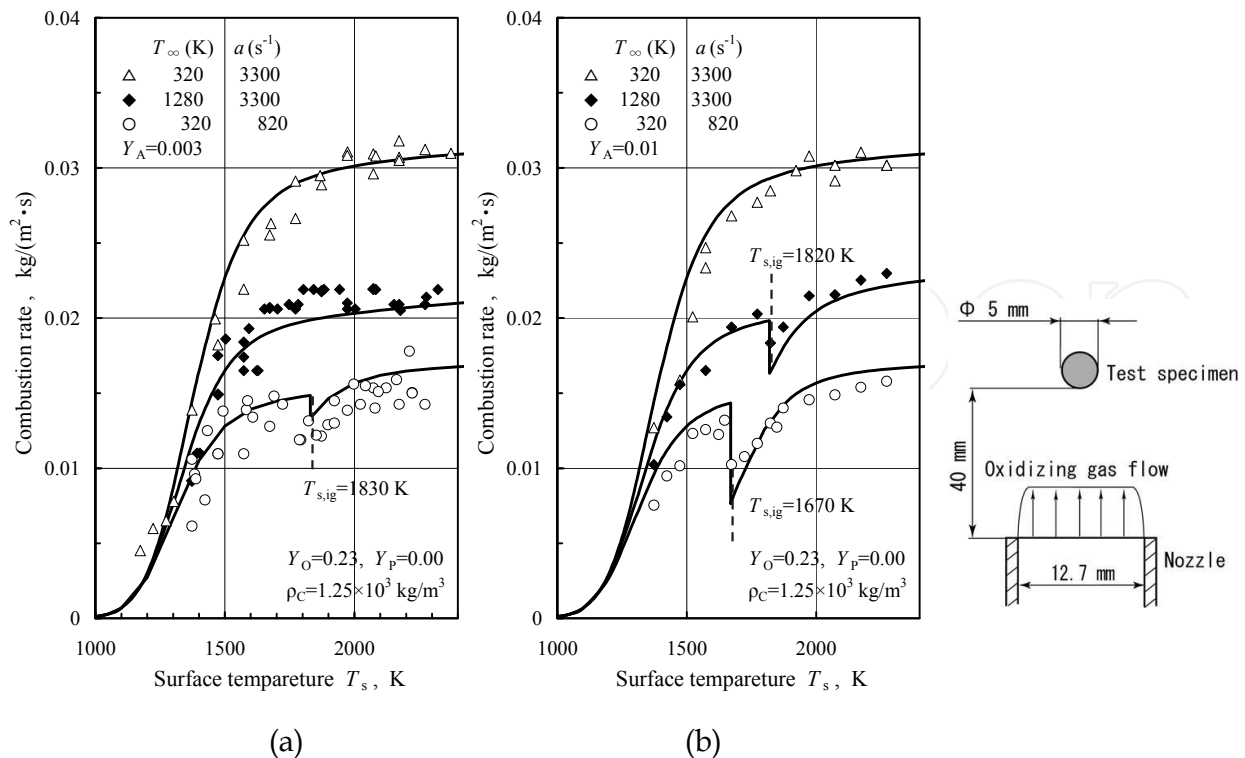


Fig. 3. Combustion rate in the high-temperature airflow with the velocity gradient $a=3300\text{ s}^{-1}$, as a function of the surface temperature T_s ; (a) for the H_2O mass-fraction $Y_A=0.003$ (Makino, et al., 2003); (b) for $Y_A=0.01$ (Makino & Umehara 2007). For comparisons, results in the room-temperature airflows with the same mass flow rate and the same velocity gradient are also shown. Data points are experimental with the test specimen of $1.25\times 10^3\text{ kg/m}^3$ in graphite density; curves are results of the explicit combustion-rate expressions. Schematical drawing of the experimental setup is also shown.

combustion rate. As for the effect of the high-temperature airflow, we can say that it promotes the combustion rate, because of the elevated transport properties (Makino, et al., 2003) that enhances the mass-transfer rate of oxidizer.

This promoting effect can also be understood by use of a functional form of the combustion rate $\dot{m} \sim (a\rho\mu)^{1/2}$, derived from Eq. (9), for the diffusion-limited conditions. In this situation, we have $a\rho = \text{const.}$ when the mass flow rates of air are the same, so that $\dot{m} \sim (\mu)^{1/2}$. Since the viscosity μ , which can also be regarded as the mass diffusivity (ρD) when the Schmidt number is unity, is elevated with increasing air temperature, the combustion rate in the high-temperature airflow is necessarily higher than that in the room-temperature airflow. Results in the room-temperature airflow with $a=3300\text{ s}^{-1}$ are also shown in Fig. 3(a). The combustion rate increases monotonically, in the same manner as that in the high-temperature airflow. Note that when the velocity gradients are the same, the combustion rate in the high-temperature airflow is lower than that in the room-temperature airflow by about 30%, because of the reduced mass-transfer rate of oxygen, due to thickened boundary layer (Makino, et al., 2003), through overcoming an increase in the mass diffusivity ($\rho D \sim \mu$). This situation can easily be understood by use of a functional form of the combustion rate $\dot{m} \sim (\mu/\delta)$, from Eq. (9), for the diffusion-limited conditions, where δ is a measure of the boundary-layer thickness, expressed as $\sim [(\mu/\rho)/a]^{1/2}$ (Schlichting, 1979).

Solid curves are theoretical (Makino, et al., 1998b; 2003). For the airflow with $a=3300 \text{ s}^{-1}$, the Frozen mode is used. For the airflow with $a=820 \text{ s}^{-1}$, up to the ignition surface-temperature predicted to be 1830 K, the Frozen mode is used, whereas the Flame-detached mode is used above the ignition surface-temperature. It is seen that a fair degree of agreement is demonstrated between experimental and theoretical results, reconfirming the appropriateness to use the Frozen and Flame-detached modes for representing the combustion behavior before and after the establishment of CO-flame, respectively.

As shown in Fig. 3(a), when the mass flow rates of airflows are the same, the combustion rate in the high-temperature airflow is enhanced, so that the advantage of this technique looks trivial. However, its quantitative evaluation is not so straightforward, because there can appear abrupt changes in the combustion rate, related to the establishment of CO-flame that depends on the H_2O mass-fraction in airflow. Furthermore, water vapor can even be an oxidizer for carbon. So, in evaluating the High-Temperature Air Combustion technique, effects of the H_2O concentration are to be examined.

3.2 Combustion in airflow with medium humidity

Figure 3(b) shows similar plots of the combustion rate when the H_2O mass-fraction $Y_A = 0.01$. Although nearly the same trends are observed, there exist slight differences. Specifically, there exists a slight decrease in the combustion rate, even in the high-temperature airflow, at about 1800 K. This can be attributed to the establishment of CO-flame, facilitated even in the fast airflow with $a=3300 \text{ s}^{-1}$, because of the increased H_2O mass-fraction. As for the combustion in the room-temperature airflow with $a=820 \text{ s}^{-1}$, the ignition surface-temperature is reduced to be about 1650 K, suggesting that the CO-flame can easily be established. Theoretical results are also shown and fair agreement is demonstrated, suggesting that the Frozen and the Flame-detached modes, respectively, represent the combustion behavior before and after the establishment of CO-flame. The ignition surface-temperature is predicted to be 1820 K for the high-temperature airflow with $a=3300 \text{ s}^{-1}$ and 1670 K for the room-temperature airflow with $a=820 \text{ s}^{-1}$, which are also in accordance with experimental observation.

3.3 Combustion in humid airflow

A further increase in the H_2O mass-fraction can considerably change the combustion behavior (Makino & Umehara, 2007). The H_2O mass-fraction Y_A is now increased to be 0.10, the dew point of which is as high as 328 K (55°C). Note that this H_2O mass-fraction is even higher than that ever used in the previous studies with humid airflow (Matsui, et al., 1983; 1986), by virtue of a small-sized boiler installed in the experimental apparatus. Figure 4(a) shows the combustion rate in the high-temperature airflow with $a=3300 \text{ s}^{-1}$, as a function of the surface temperature T_s . The O_2 mass-fraction is reduced, because of the increased H_2O concentration. It is seen that the combustion rate increases first gradually and then rapidly with increasing surface temperature. This trend is quite different from that in Figs. 3(a) or 3(b).

In order to elucidate causes for this trend, theoretical results are obtained, with additional surface C- H_2O and global gas-phase H_2 - O_2 reactions taken into the formulation (Makino & Umehara, 2007), which will be explained later. Not only results in the Frozen and Flame-detached modes, but also that in the Flame-attached mode is shown. In the Flame-attached mode, it is assumed that combustion products of the surface reactions can immediately be

oxidized, so that neither CO nor H₂ is ejected into the gas phase. It is seen that experimental results at temperatures lower than about 1500 K are close to the theoretical result of the Flame-attached mode, while those at temperatures higher than about 1700 K are close to the result of the Flame-detached mode. The ignition surface-temperature is predicted to be 1380 K. From these comparisons, we can deduce that because of the high H₂O mass-fraction, as well as the high-temperature airflow, the CO-flame established at 1380 K adheres to the carbon surface. The combustion in the Flame-attached mode prevails until CO-ejection becomes strong enough to separate the CO-flame from the surface. As the surface temperature is increased, the CO-flame detaches, so that the combustion proceeds in the Flame-detached mode. The rapid increase in the combustion rate at high temperatures can be attributed to the participation of the C-H₂O reaction.

Figure 4(b) shows the combustion rate in the room-temperature airflow with the same mass flow rate ($a=820\text{ s}^{-1}$). The airflow temperature, being raised to $T_\infty=370\text{ K}$ for preventing condensation of water vapor, cannot be called as the "room" temperature, any more, but its terminology is retained to distinguish it from the high-temperature. It is seen that the combustion rate gradually increases with increasing surface temperature. Compared to Fig. 4(a), the combustion rate around 1500 K is nearly the same as that in the high-temperature airflow. So, we can say that when the H₂O concentration is high, there is no merit to use the high-temperature airflow, until the water vapor begins to participate in the surface reaction as another oxidizer at about 1700 K or higher. A difference in the combustion rates at high temperatures becomes large because no remarkable increase in the combustion rate is observed, although the water vapor is anticipated to participate in the surface reaction. A further consideration will be made later.

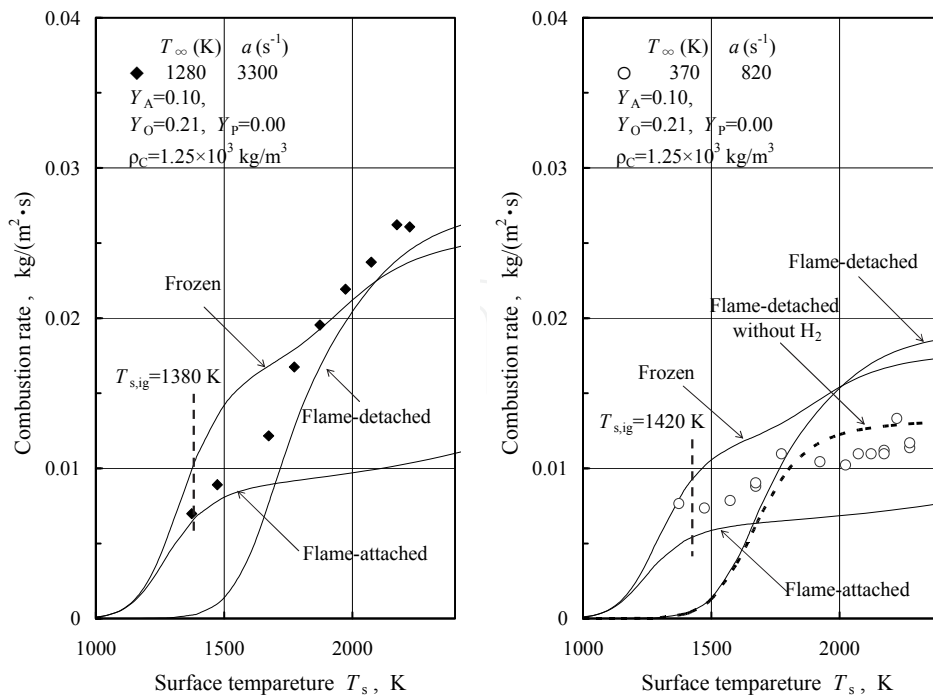
Theoretical results are also shown in Fig. 4(b). The ignition surface-temperature is now predicted to be 1420 K. We see that the combustion rate experimentally obtained locates in the middle of the theoretical results in the Frozen and Flame-attached modes, after the establishment of CO-flame, suggesting that the gas-phase reaction proceeds in a finite rate, because the airflow is neither fast in velocity nor high in temperature. One more thing to be noted is the combustion behavior at high temperatures, presenting that the combustion rate in the experiment cannot reach the theoretical result that the Flame-detached mode predicts, about which it will be discussed later.

Figure 4(c) shows the combustion rate in the room-temperature airflow with $a=3300\text{ s}^{-1}$. Nearly the same trend as that in Figs. 3(a) and/or 3(b) with low velocity gradient is shown. Because the airflow temperature is low, the establishment of CO-flame is retarded until the surface temperature reaches about 1700 K, and the combustion rate up to this temperature is about double of that in the high-temperature airflow. The rapid increase at high temperatures can be attributed to the contribution of the surface C-H₂O reaction.

Theoretical results are also shown in Fig. 4(c). Until the establishment of CO-flame at $T_s = 1690\text{ K}$ predicted, we see again that the Frozen mode can fairly represent the combustion behavior. At high temperatures at which the CO-flame has already been established, the combustion behavior is fairly represented by the Flame-detached mode.

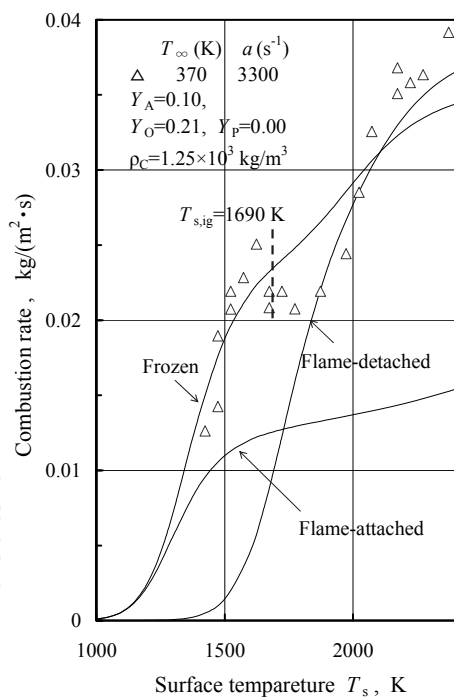
4. Extended formulation for the carbon combustion

Theoretical study (Makino & Umehara, 2007) has been conducted for the system with three surface reactions and two global gas-phase reactions, by extending the previous formulation. Although some of the assumptions introduced in Section 2 in Part 1 are not



(a)

(b)



(c)

Fig. 4. Combustion rate in humid airflow (Makino & Umehara, 2007) with the H_2O mass-fraction $Y_A=0.10$, as a function of the surface temperature T_s ; (a) in the high-temperature airflow with the velocity gradient $a=3300 \text{ s}^{-1}$; (b) in the room-temperature airflow with the same mass flow rate ($a=820 \text{ s}^{-1}$); (c) in the room-temperature airflow with the same velocity gradient. Data points are experimental and curves are results of the explicit combustion-rate expressions.

appropriate for systems with hydrogen species, use has been made of those as they are, for tractability, in order to capture fundamental aspects of the carbon combustion under prescribed situations.

4.1 Mass fractions of oxidizers at the carbon surface

By extending Eq. (31) in Part 1, so as to include contribution of the C-H₂O reaction, the combustion rate ($-f_s$) can be expressed as

$$\delta(-f_s) = A_{s,O} \tilde{Y}_{O,s} + A_{s,P} \tilde{Y}_{P,s} + A_{s,A} \tilde{Y}_{A,s}. \quad (20)$$

Again, use has been made of an assumption that all the surface reactions are the first-order. The reduced surface Damköhler number $A_{s,i}$, the surface Damköhler number $Da_{s,i}$ and the stoichiometrically weighted mass fraction, relevant to the oxidizing species i ($=O, P, A$) are also defined in the same manner as those in Section 2 in Part 1.

Although $Y_{i,s}$ must be determined through numerical calculations when the gas-phase kinetics is finite, they can be determined analytically for some limiting cases, as mentioned. One of them is the **Frozen mode**, in which we have

$$\tilde{Y}_{i,s} = \frac{Y_{i,\infty}}{1 + \beta + A_{s,i} [\beta / (-f_s)]} \quad (i = O, P, A). \quad (21)$$

Another is the **Flame-attached mode** in which CO and H₂ produced at the surface reactions are immediately consumed, so that it looks that the CO-flame adheres to the surface. In the same manner (Makino, et al., 1998b), we have

$$\tilde{Y}_{O,s} = \frac{\tilde{Y}_{O,\infty} - 2\delta\beta}{1 + \beta}, \quad \tilde{Y}_{P,s} = \frac{\tilde{Y}_{P,\infty} + \delta\beta}{1 + \beta}, \quad \tilde{Y}_{A,s} = \frac{\tilde{Y}_{A,\infty}}{1 + \beta}. \quad (22)$$

The third is the **Flame-detached mode** in which the gas-phase reaction is infinitely fast and the CO-flame locates in the gas phase. Although a coupling function

$$\tilde{Y}_{O,s} + \tilde{Y}_{P,s} + \tilde{Y}_{A,s} = \frac{\tilde{Y}_{O,\infty} + \tilde{Y}_{P,\infty} + \tilde{Y}_{A,\infty} - \delta\beta}{1 + \beta} \quad (23)$$

can easily be obtained and we can also put $Y_{O,s} = 0$ for this combustion situation, a separation of $Y_{A,s}$ from $Y_{P,s}$ is not straightforward. For this aim, it is needed to take account of another species-enthalpy coupling function, say, (Makino & Umehara, 2007)

$$\tilde{T} + \tilde{Y}_O + (1 - \tilde{Q})\tilde{Y}_A, \quad (24)$$

then we have

$$\tilde{Y}_{A,s} = \frac{1}{1 - \tilde{Q}} \frac{\tilde{T}_\infty - \tilde{T}_s + \tilde{Y}_{O,\infty} + (1 - \tilde{Q})\tilde{Y}_{A,\infty} - \gamma}{1 + \beta + A_{s,A} [\beta / (-f_s)]}. \quad (25)$$

Here, \tilde{Q} is the ratio of the heats of combustion of the H_2-O_2 and $CO-O_2$ reactions in the gas phase. For evaluating γ , the temperature profile $T = T_s + (T_f - T_s)(\xi/\xi_f)$ inside the flame has been used, so that we have

$$\gamma = \tilde{T}_\infty - \tilde{T}_s + \tilde{Y}_{O,\infty} + (1 - \tilde{Q})\tilde{Y}_{A,\infty} + (1 - \tilde{Q}) \left(\tilde{Y}_{A,s} \frac{1 - \xi_f}{\xi_f} - \frac{\tilde{Y}_{A,f}}{\xi_f} \right), \quad (26)$$

where the coupling function in Eq. (24) is evaluated at the flame. By further using ξ_f and $Y_{A,f}$, determined by use of other coupling functions $\tilde{Y}_O - \tilde{Y}_F - \tilde{Y}_H$ and $\tilde{Y}_H + \tilde{Y}_A$, respectively, we have from Eq. (25) as

$$\tilde{Y}_{A,s} = \frac{\tilde{Y}_{A,\infty}}{1 + \beta + A_{s,A} \frac{\beta}{(-f_s)} \left(1 - \frac{\tilde{Y}_{O,\infty}}{2\delta\beta} \right)}. \quad (27)$$

The other mode that has been found (Makino & Umehara, 2007) is the **Flame-detached mode without H_2** , in which there exists no H_2 in the gas phase because it can easily be oxidized. For this mode, we have

$$\tilde{Y}_{O,s} = 0, \quad \tilde{Y}_{P,s} = \frac{\tilde{Y}_{O,\infty} + \tilde{Y}_{P,\infty} - \delta\beta}{1 + \beta}, \quad \tilde{Y}_{A,s} = \frac{\tilde{Y}_{A,\infty}}{1 + \beta}, \quad (28)$$

4.2 Approximate, explicit expressions for the combustion rate

By use of the approximate relation in Eq. (4), analytical expressions for β can be obtained as

(I) Frozen mode:

$$\beta \approx \left(\frac{KA_{s,O}}{1 + KA_{s,O}} \right) \left(\frac{2W_C}{W_O} Y_{O,\infty} \right) + \left(\frac{KA_{s,P}}{1 + KA_{s,P}} \right) \left(\frac{W_C}{W_P} Y_{P,\infty} \right) + \left(\frac{KA_{s,A}}{1 + KA_{s,A}} \right) \left(\frac{W_C}{W_A} Y_{A,\infty} \right), \quad (29)$$

(II) Flame-attached mode:

$$\beta \approx \left(\frac{1}{1 + 2KA_{s,O} - KA_{s,P}} \right) \left(KA_{s,O} \frac{2W_C}{W_O} Y_{O,\infty} + KA_{s,P} \frac{W_C}{W_P} Y_{P,\infty} + KA_{s,A} \frac{W_C}{W_A} Y_{A,\infty} \right), \quad (30)$$

(III) Flame-detached mode:

$$\beta \approx \frac{1}{2} \left\{ \frac{KA_{s,P}}{1 + KA_{s,P}} \left(\frac{2W_C}{W_O} Y_{O,\infty} + \frac{W_C}{W_P} Y_{P,\infty} \right) + \frac{KA_{s,A}}{1 + KA_{s,A}} \left(\frac{W_C}{W_O} Y_{O,\infty} + \frac{W_C}{W_A} Y_{A,\infty} \right) \right\} \\ + \frac{1}{2} \left[\left\{ \frac{KA_{s,P}}{1 + KA_{s,P}} \left(\frac{2W_C}{W_O} Y_{O,\infty} + \frac{W_C}{W_P} Y_{P,\infty} \right) - \frac{KA_{s,A}}{1 + KA_{s,A}} \left(\frac{W_C}{W_O} Y_{O,\infty} + \frac{W_C}{W_A} Y_{A,\infty} \right) \right\}^2 \right]$$

$$+ 4 \frac{KA_{s,P}}{1 + KA_{s,P}} \left(\frac{W_C}{W_O} Y_{O,\infty} + \frac{W_C}{W_P} Y_{P,\infty} \right) \frac{KA_{s,A}}{1 + KA_{s,A}} \left(\frac{W_C}{W_A} Y_{A,\infty} \right) \Bigg]^{1/2}, \quad (31)$$

(IV) Flame-detached mode without H₂:

$$\beta \approx \left(\frac{KA_{s,P}}{1 + KA_{s,P}} \right) \left(\frac{2W_C}{W_O} Y_{O,\infty} + \frac{W_C}{W_P} Y_{P,\infty} \right) + \left(\frac{KA_{s,A}}{1 + KA_{s,P}} \right) \left(\frac{W_C}{W_A} Y_{A,\infty} \right). \quad (32)$$

As the correction factor K for the two-dimensional flow, we have Eq. (16) for the Frozen and Flame-attached modes; Eq. (18) for the Flame-detached mode, regardless of H₂ ejection from the carbon surface.

4.3 Surface kinetic parameters and thermophysical properties

In numerical calculations, use has been made of the kinetic parameters for the surface C-O₂ and C-CO₂ reactions, described in Section 5 in Part 1. For C-H₂O reaction, the frequency factor $B_{s,A}=2 \times 10^7$ m/s and activation energy $E_{s,A}=271$ kJ/mol, determined after re-examining previous experimental results (Makino, et al., 1998a). As mentioned, effects of porosity and/or other surface characteristics are grouped into the kinetic parameters. Thermophysical properties are $\rho_\infty=1.10$ kg/m³ and $\mu_\infty=1.95 \times 10^{-5}$ Pa·s for the room-temperature airflow ($T_\infty=320$ K), while $\rho_\infty=0.276$ kg/m³ and $\mu_\infty=5.10 \times 10^{-5}$ Pa·s for the high-temperature airflow ($T_\infty=1280$ K). As for the thermophysical properties of water vapor, $\rho_\infty=0.598$ kg/m³ and $\mu_\infty=1.22 \times 10^{-5}$ Pa·s at $T_\infty=370$ K. Wilke's equation (Reid, et al., 1977) has been used in estimating viscosities of humid air.

4.4 Further consideration for experimental comparisons

Experimental results have already been compared with theoretical results in Figs. 3 and 4, and a fair degree of agreement has been demonstrated in general, suggesting appropriateness of the analysis, including the choice of the thermophysical properties. However, Fig. 4(b) requires a further comment because theoretical result of the Flame-detached mode overestimates the combustion rate, especially at high surface temperatures T_s . As assumed in the Flame-detached mode, CO and H₂ produced at the surface reaction are to be transported to the flame and then oxidized. Generally speaking, however, H₂ can easily be oxidized, compared to CO, especially at high temperatures. In addition, the velocity gradient ($a=820$ s⁻¹) in Fig. 4(b) is not so high. In this situation, H₂ produced at the surface reaction is considered to be completely consumed by the water-gas shift reaction ($H_2+CO_2 \rightarrow H_2O+CO$), so that the Flame-detached mode without H₂ presented (Makino & Umehara, 2007) seems to be appropriate. A theoretical result is also shown in Fig. 4(b) by a dashed curve. We see that the agreement at high T_s has much been improved, suggesting that this consideration is to the point.

5. Other results relevant to the high-temperature air combustion

As one of the advantages for the High-Temperature Air Combustion, it has been pointed out that oxygen concentration in a furnace can be reduced without reducing combustion rate. In order to confirm this fact, an experiment has been conducted by varying O₂ and CO₂ concentrations in the high-temperature oxidizer-flow (Makino and Umehara, 2007). In

addition, combustion rate of C/C-composite in the high-temperature airflow has been examined (Makino, et al., 2006) in a similar way, relevant to evaluation of protection properties from oxidation. In this Section, those results not presented in previous Sections are shown.

5.1 Effects of O₂ and CO₂ in the oxidizer-flow

Experimental conditions for the O₂ and/or CO₂ concentrations in the high-temperature oxidizer-flow have been chosen to have the same combustion rate as that in the room-temperature airflow, at around $T_s=2000$ K, shown in Fig. 3(a). Figure 5(a) shows the combustion rate in the high-temperature oxidizer-flow, as a function of the surface temperature T_s . The O₂ and CO₂ mass-fractions are set to be 0.105 and 0.10, respectively. The H₂O mass-fraction $Y_A=0.001$ or less. Because of the monotonic increase in the combustion rate, the combustion rate at 2000 K is nearly equal to that in the room-temperature airflow, shown in Figs. 3(a) and 3(b), experienced the abrupt decreases in the combustion rate upon the establishment of CO-flame, although it is generally suppressed, because of the reduced O₂ mass-fraction. For comparisons, results in the room-temperature oxidizer-flows with the same mass flow rate and the same velocity gradient are also shown in Fig. 5(a), the general trend of which is in accordance with that in the airflow shown in Figs. 3(a) and 3(b), as far as the combustion rate is concerned.

Figure 5(b) shows the combustion rate as a function of T_s , with CO₂ taken as the only oxidizer. The CO₂ mass-fraction is set to be 0.39. Since CO₂ is the only oxidizer for the

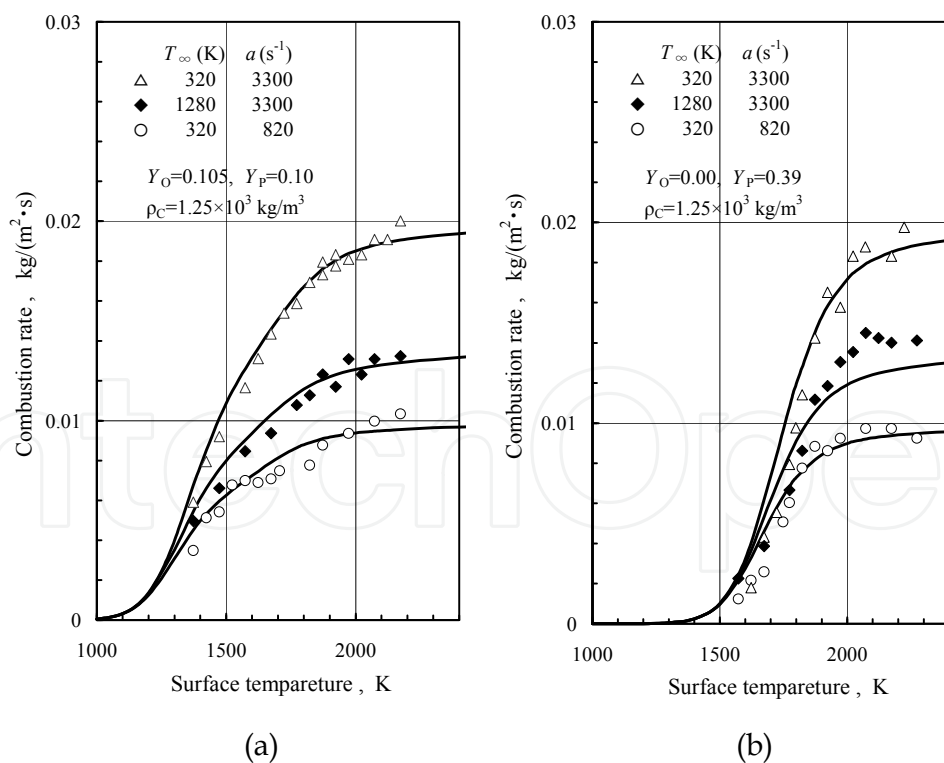


Fig. 5. Combustion rate in the high-temperature oxidizer-flow with the velocity gradient $a = 3300 \text{ s}^{-1}$, as a function of the surface temperature (Makino and Umehara, 2007). The H₂O mass-fraction $Y_A=0.001$ or less. Notation is the same as that in Fig. 3. (a) The O₂ and CO₂ mass-fractions are 0.105 and 0.10, respectively; (b) The CO₂ mass-fraction is 0.39.

surface reaction and there is no gas phase reaction, the monotonic increase in the combustion rate is observed. The same comments as those in Fig. 3(a) can be made for the high-temperature oxidizer-flow although higher surface temperature T_s is required in activating the surface C-CO₂ reaction.

Finally, it is confirmed that as far as the combustion rates at around $T_s=2000$ K are concerned, those in the high-temperature oxidizer-flows in Figs. 5(a) and 5(b) are nearly the same as that in the room-temperature airflow in Fig. 3(a) with the same mass flow rate. As pointed out (Makino, et al., 2003) that the O₂ mass-fraction can be reduced down to about 0.14 in the High-Temperature Air Combustion, without reducing combustion rate, it has been confirmed that the O₂ mass-fraction can further be reduced (Makino and Umehara, 2007) when there exists CO₂ in the oxidizer-flow.

5.2 Combustion rate of C/C-composite

Figure 6(a) shows the combustion rate as a function of the surface temperature with the velocity gradient taken as a parameter. Use has been made of a test specimen of C/C-composite with rectangular cross section (5 mm width; 8 mm thickness). The velocity gradient used here is defined as $a = 2V_\infty/\ell$, where ℓ is the width; the maximum velocity gradient is limited to be 1300 s⁻¹, because of air-supply system. Other experimental conditions are the same as those in Figs. 1(a) and/or 3(a). An abrupt decrease in the combustion rate, as well as the general combustion response can be observed in the same manner as that of a graphite rod, reported in the previous Sections. Figure 6(b) is a similar plot with the airflow temperature taken as a parameter, presenting the same trend as that in Fig. 3(a).

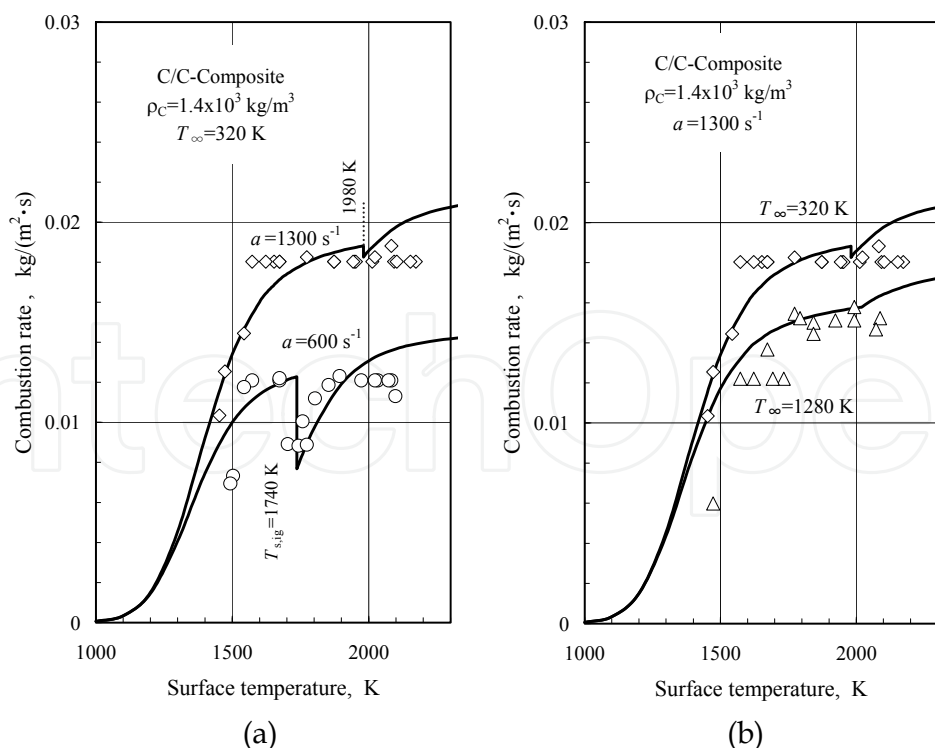


Fig. 6. Combustion rate of C/C-composite (Makino, et al., 2006) as a function of the surface temperature; (a) with the velocity gradient of airflow taken as a parameter; (b) with the airflow temperature taken as a parameter.

Theoretical results are also shown in Figs. 6(a) and 6(b). In obtaining these results, use has been made of kinetic parameters for the artificial graphite with higher density ($\rho_C = 1.82 \times 10^3$ kg/m³), after confirming the experimental fact that there appears no remarkable difference in the combustion rates in different graphite densities, because of the prevalence of combustion behavior in the diffusionaly controlled regime in the present experimental conditions. As far as the trend and approximate magnitude are concerned, fair agreement is demonstrated, including the ignition surface-temperature. It should be noted that the combustion rate of the C/C-composite is nearly the same as that of artificial graphite when there is no surface coating for protecting oxidation.

6. Concluding remarks

In this monograph, combustion of solid carbon has been overviewed not only experimentally but also theoretically. As explained in Part 1, only the carbon combustion in the forward stagnation flowfield has been considered, in order to have a clear understanding.

In Part 1, by conducting the aerothermochemical analysis, based on the chemically reacting boundary layer, with considering the surface C-O₂ and C-CO₂ reactions and the gas-phase CO-O₂ reaction, the generalized species-enthalpy coupling functions have successfully been derived, which demonstrate close coupling between the surface and gas-phase reactions that can also exert influences on the combustion rate.

Then, focus has been put on the ignition of CO-flame over the burning carbon in the prescribed flowfield, because establishment of the CO-flame in the gas phase can change the dominant surface reaction from the faster C-O₂ reaction to the slower C-CO₂ reaction, causing abrupt changes in the combustion rate. By further conducting the asymptotic expansion analysis, with using the generalized coupling functions, the explicit ignition criterion has been derived, suggesting that ignition is facilitated with increasing surface temperature and oxidizer concentration, while suppressed with decreasing velocity gradient.

Then, attempts have been made to estimate kinetic parameters for the surface and gas-phase reactions, indispensable for predicting combustion behavior, with using theoretical results obtained. A fair degree of agreement has been demonstrated between experimental and theoretical results, through conducting experimental comparisons.

In Part 2, a further study has been conducted in the stagnation flow with high velocity gradient, at least one order of magnitude higher than that ever used, in order to suppress the appearance of CO-flame. It is observed that the combustion rate increases monotonically and reaches the diffusion-limited value with increasing surface temperature when the velocity gradient is high, while there exists a discontinuous change in the combustion rate with increasing surface temperature, due to the establishment of CO-flame when the velocity gradient is low. In addition, an attempt has been made to obtain explicit combustion-rate expressions, presented by the transfer number in terms of the natural logarithmic term, just like that for droplet combustion. For the three limiting cases, explicit expressions have further been obtained by making an assumption of small combustion rate. It has even been found that before the establishment of CO-flame the combustion rate can fairly be represented by the expression in the Frozen mode, and that after the establishment of CO-flame the combustion rate can be represented by the expression in the Flame-attached and/or Flame-detached modes. Since the present expressions are explicit and have fair

accuracy, they are anticipated to make various contributions not only for qualitative and quantitative studies in facilitating understanding, but also for practical utility, such as designs of furnaces, combustors, ablative carbon heat-shields, and high-temperature structures with C/C-composites in various aerospace applications.

Finally, relevant to the High-Temperature Air Combustion, carbon combustion has been studied, by varying H₂O mass-fraction up to 0.10. It has been found that the high H₂O mass-fraction is unfavorable for the enhancement of combustion rate, especially in the medium temperature range, because establishment of the CO-flame is facilitated, and hence suppresses the combustion rate. To the contrary, at high surface temperatures (>2000 K), the high H₂O mass-fraction is favorable because the water vapor participates in the surface reaction as an additional oxidizer. Theoretical results, obtained by additionally introducing the surface C-H₂O reaction and the global gas-phase H₂-O₂ reaction into the previous formulation, have also suggested the usefulness of the explicit expressions for the combustion rate. As for the combustion in the humid airflow with relatively low velocity gradient, it is found that a new mode with suppressed H₂-ejection from the surface can fairly represent the experimental observation.

Although essential feature of the carbon combustion has been captured to some extents, further progresses are strongly required for its firm understanding, because wide attention has been given to carbonaceous materials in various fields.

7. Acknowledgment

In conducting a series of studies on the carbon combustion, I have been assisted by many of my former graduate and undergraduate students, as well as research staffs, in Shizuoka University, being engaged in researches in the field of mechanical engineering for twenty years as a staff, from a research associate to a full professor. Here, I want to express my sincere appreciation to all of them who have participated in researches for exploring combustion of solid carbon.

8. Nomenclature

A	reduced surface Damköhler number
a	velocity gradient in the stagnation flowfield
B	frequency factor
b	constant
c	constant
c_p	specific heat capacity of gas
D	diffusion coefficient
Da	Damköhler number
d	diameter or constant
E	activation energy
F	function defined in the ignition criterion
f	nondimensional streamfunction
h_D	mass-transfer coefficient
j	$j=0$ and 1 designate two-dimensional and axisymmetric flows, respectively
K	factor
k	surface reactivity

L	convective-diffusive operator
l	width
\dot{m}	dimensional mass burning (or combustion) rate
Q	ratio of heats of combustion in the gas phase
q	heat of combustion per unit mass of CO
R^o	universal gas constant
R	curvature of surface or radius
s	boundary-layer variable along the surface
T	temperature
T_a	activation temperature
t	time
u	velocity component along x
V	freestream velocity
v	velocity component along y
W	molecular weight
w	reaction rate
x	tangential distance along the surface
Y	mass fraction
y	normal distance from the surface

Greek Symbols

α	stoichiometric CO ₂ -to-reactant mass ratio
β	conventional transfer number
γ	temperature gradient at the surface
Δ	reduced gas-phase Damköhler number
δ	product(CO ₂)-to-carbon mass ratio or boundary-layer thickness
ε	measure of the thermal energy in the reaction zone relative to the activation energy
η	boundary-layer variable normal to the surface or perturbed concentration
Θ	perturbed temperature in the outer region
θ	perturbed temperature in the inner region
λ	thermal conductivity or parameter defined in the ignition analysis
μ	viscosity
ν	stoichiometric coefficient
ξ	profile function
ρ	density
χ	inner variable
ψ	streamfunction
ω	reaction rate

Subscripts

A	water vapor or C-H ₂ O surface reaction
a	critical value at flame attachment
C	carbon
F	carbon monoxide
f	flame sheet

g	gas phase
ig	ignition
in	inner region
max	maximum value
N	nitrogen
O	oxygen or C-O ₂ surface reaction
out	outer region
P	carbon dioxide or C-CO ₂ surface reaction
s	surface
∞	freestream or ambience

Superscripts

<i>a</i>	reaction order
<i>j</i>	<i>j</i> =0 and 1 designate two-dimensional and axisymmetric flows, respectively
~	nondimensional or stoichiometrically weighted
'	differentiation with respect to η
*	without water-vapor effect

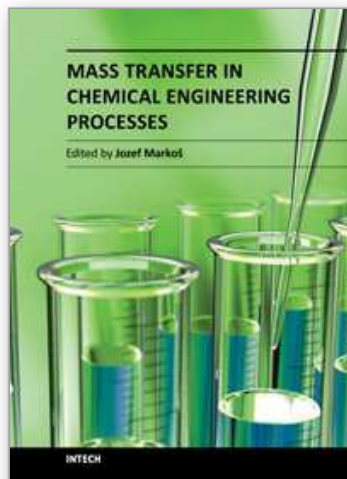
9. References

- Annamalai, K. & Ryan, W. (1993). Interactive Processes in Gasification and Combustion-II. Isolated Carbon, Coal and Porous Char Particles. *Prog. Energy Combust. Sci.*, Vol. 19, No. 5, pp. 383-446, ISSN 0360-1285.
- Annamalai, K., Ryan, W., & Dhanapalan, S. (1994). Interactive Processes in Gasification and Combustion-Part III: Coal/Char Particle Arrays, Streams and Clouds. *Prog. Energy Combust. Sci.*, Vol. 20, No. 6, pp. 487-618, ISSN 0360-1285.
- Batchelder, H. R., Busche, R. M., & Armstrong, W. P. (1953). Kinetics of Coal Gasification. *Ind. Eng. Chem.*, Vol. 45, No. 9, pp. 1856-1878.
- Chung, P. M. (1965). Chemically Reacting Nonequilibrium Boundary Layers. In: *Advances in Heat Transfer*, Vol. 2, J. P. Hartnett, & T. F. Irvine, Jr. (Eds.), Academic, pp. 109-270, ISBN 0-12-020002-3, New York.
- Clark, T. J., Woodley, R. E., & De Halas, D. R. (1962). Gas-Graphite Systems, In: *Nuclear Graphite*, R. E. Nightingale (Ed.), pp.387-444, Academic, New York.
- Essenhigh, R. H. (1976). Combustion and Flame Propagation in Coal Systems: A Review. *Proc. Combust. Inst.*, Vol. 16, No. 1, pp. 353-374, ISSN 0082-0784.
- Essenhigh, R. H. (1981). Fundamentals of Coal Combustion, In: *Chemistry of Coal Utilization*, M. A. Elliott (Ed.), pp. 1153-1312, Wiley-Interscience, ISBN 0-471-07726-7, New York.
- Fischbeck, K. (1933). Über das Reaktionsvermögen der Festen Stoffe. *Z. Elektrochem.*, Vol. 39, No. 5, pp. 316-330.
- Fischbeck, K., Neundeubel, L. & Salzer, F. (1934). Über das Reaktionsvermögen von Kristallarten. *Z. Elektrochem.*, Vol. 40, No. 7b, pp. 517-522.
- Frank-Kamenetskii, D. A. (1969). *Diffusion and Heat Transfer in Chemical Kinetics*, 2nd Enlarged/Revised Ed., J. P. Appleton (Translation Ed.), Plenum, ISBN0-306-30349-3, New York.

- Gerstein, M. & Coffin, K. P. (1956). Combustion of Solid Fuels, In: *Combustion Processes*, B. Lewis, R. N. Pease, and H. S. Taylor (Eds.), Princeton UP, Princeton, pp.444-469.
- Katsuki, M. & Hasegawa, T. (1998). The Science and Technology of Combustion in Highly Preheated Air. *Proc. Combust. Inst.*, Vol. 27, No. 2, pp. 3135-3146, ISSN 0082-0784
- Katto, Y. (1982a). *An Outline of Heat Transfer*, Yoken-do, Tokyo.
- Khitrin, L. N. (1962). *The Physics of Combustion and Explosion*, Israel Program for Scientific Translations, Jerusalem.
- Law, C. K. (1978). On the Stagnation-Point Ignition of a Premixed Combustion. *Int. J. Heat Mass Transf.*, Vol. 21, No. 11, pp. 1363-1368, ISSN 0017-9310.
- Maahs, H. G. (1971). Oxidation of Carbon at High Temperatures: Reaction-Rate Control or Transport Control. NASA TN D-6310.
- Makino, A. (1990). A Theoretical and Experimental Study of Carbon Combustion in Stagnation Flow. *Combust. Flame*, Vol. 81, No. 2, pp. 166-187, ISSN 0010-2180.
- Makino, A. (1992). An Approximate Explicit Expression for the Combustion Rate of a small Carbon Particle. *Combust. Flame*, Vol. 90, No. 2, pp. 143-154, ISSN 0010-2180.
- Makino, A. & Law, C. K. (1990). Ignition and Extinction of CO Flame over a Carbon Rod. *Combust. Sci. Technol.*, Vol. 73, No. 4-6, pp. 589-615, ISSN 0010-2202.
- Makino, A. & Umehara, N. (2007). Combustion Rates of Graphite Rods in the Forward Stagnation Field of the High-Temperature, Humid Airflow. *Proc. Combust. Inst.*, Vol. 31, No. 2, pp. 1873-1880, ISSN 1540-7489.
- Makino, A., Araki, N., & Mihara, Y. (1994). Combustion of Artificial Graphite in Stagnation Flow: Estimation of Global Kinetic Parameters from Experimental Results. *Combust. Flame*, Vol. 96, No. 3, pp. 261-274, ISSN 0010-2180.
- Makino, A., Fujizaki, H., & Araki, N. (1998a). Combustion Rate of Burning Graphite in a Stagnation Flow of Water Vapor. *Combust. Flame*, Vol. 113, No. 1-2, pp. 258-263, ISSN 0010-2180.
- Makino, A., Kato, I., Senba, M., Fujizaki, H., & Araki, N. (1996). Flame Structure and Combustion Rate of Burning Graphite in the Stagnation Flow. *Proc. Combust. Inst.*, Vol. 26, No. 2, pp. 3067-3074, ISSN 0082-0784.
- Makino, A., Namikiri, T., & Araki, N. (1998b). Combustion Rate of Graphite in a High Stagnation Flowfield and Its Expression as a Function of the Transfer Number. *Proc. Combust. Inst.*, Vol. 27, No. 2, pp. 2949-2956, ISSN 0082-0784.
- Makino, A., Namikiri, T., & Kimura, K. (2003). Combustion Rates of Graphite Rods in the Forward Stagnation Field with High Temperature Airflow. *Combust. Flame*, Vol. 132, No. 4, pp. 743-753, ISSN 0010-2180.
- Makino, A., Namikiri, T., & Kimura, K. (2006). Combustion of Solid Carbon with High Density and Carbon/Carbon-Composite in the Stagnation Flow Field. *Trans. Jpn. Soc. Mech. Eng. (Series B)*, Vol. 72, No. 724, pp. 3137-3142, ISSN 0387-5016. [in Japanese].
- Matsui, K., Kôyama, A., & Uehara, K. (1975). Fluid-Mechanical Effects on the Combustion Rate of Solid Carbon. *Combust. Flame*, Vol. 25, No. 1, pp. 57-66, ISSN 0010-2180.
- Mulcahy, M. F. & Smith, I. W. (1969). Kinetics of Combustion of Pulverized Fuel: A Review of Theory and Experiment. *Rev. Pure and Appl. Chem.*, Vol. 19, No. 1, pp. 81-108.
- Nagel, J. & Strickland-Constable, R. F. (1962). Oxidation of Carbon between 1000-2000°C. *Proc. Fifth Conf. On Carbon*, pp. 154-164, Pergamon, New York.

- Reid, R. C., Prausnitz, J. M., & Sherwood, T. K. (1977). Viscosities of Gas Mixtures at Low Pressures. *The Properties of Gases and Liquid, 3rd Ed.*, pp. 410-414, McGraw-Hill, ISBN 0-07-051790-8, New York.
- Rosner, D. E. (1972). High-Temperature Gas-Solid Reactions, *Annual Review of Materials Science*, Vol. 2, pp. 573-606, ISSN 0084-6600.
- Schlichting, H. (1979). *Boundary-Layer Theory, Seventh Ed.*, McGraw-Hill, ISBN 0-07-055334-3, New York.
- Spalding, D. B. (1951). Combustion of Fuel Particles. *Fuel*, Vol. 30, No. 1, pp. 121-130, ISSN 0016-2361
- Tsuji, H., Gupta, A. K., Hasegawa, T., Katsuki, M., Kishimoto, K., & Morita, M. (2003). *High Temperature Air Combustion from Energy Conservation to Pollution Reduction*, CRC Press, ISBN 0-8493-1036-9, Boca Raton.
- Tu, C. M., Davis, H., & Hottel, H. C. (1934). Combustion Rate of Carbon; Combustion of Spheres in Flowing Gas Streams. *Ind. Eng. Chem.*, Vol. 26, No. 7, pp. 749-757.
- Visser, W. & Adomeit, G. (1984). Experimental Investigation of the Ignition and Combustion of a Graphite Probe in Cross Flow. *Proc. Combust. Inst.*, Vol. 20, No. 2, pp. 1845-1851, ISSN 0082-0784.
- Walker, P. L., Jr., Rusinko, F., Jr., & Austin, L. G. (1959). Gas Reaction of Carbon, In: *Advances in Catalysis and Related Subjects*, Vol. 11, D. D. Eley, P. W. Selwood, & P. B. Weisz (Eds.), pp. 133-221, Academic, ISBN 0-12-007811-2, New York.
- White, F. M. (1988). *Heat and Mass Transfer*, Addison-Wesley, ISBN 0-201-17099-X, Reading.
- Yang, R. T. & Steinberg, M. (1977). A Diffusion Cell Method for Studying Heterogeneous Kinetics in the Chemical Reaction/Diffusion Controlled Region. Kinetics of $C + CO_2 \rightarrow 2CO$ at 1200-1600°C. *Ind. Eng. Chem. Fundam.*, Vol. 16, No. 2, pp. 235-242, ISSN 0196-4313.

IntechOpen



Mass Transfer in Chemical Engineering Processes

Edited by Dr. Jozef Marko

ISBN 978-953-307-619-5

Hard cover, 306 pages

Publisher InTech

Published online 04, November, 2011

Published in print edition November, 2011

This book offers several solutions or approaches in solving mass transfer problems for different practical chemical engineering applications: measurements of the diffusion coefficients, estimation of the mass transfer coefficients, mass transfer limitation in separation processes like drying, extractions, absorption, membrane processes, mass transfer in the microbial fuel cell design, and problems of the mass transfer coupled with the heterogeneous combustion. I believe this book can provide its readers with interesting ideas and inspirations or direct solutions of their particular problems.

How to reference

In order to correctly reference this scholarly work, feel free to copy and paste the following:

Atsushi Makino (2011). Mass Transfer Related to Heterogeneous Combustion of Solid Carbon in the Forward Stagnation Region - Part 2 - Combustion Rate in Special Environments, Mass Transfer in Chemical Engineering Processes, Dr. Jozef Marko (Ed.), ISBN: 978-953-307-619-5, InTech, Available from: <http://www.intechopen.com/books/mass-transfer-in-chemical-engineering-processes/mass-transfer-related-to-heterogeneous-combustion-of-solid-carbon-in-the-forward-stagnation-region-2>

INTECH

open science | open minds

InTech Europe

University Campus STeP Ri
Slavka Krautzeka 83/A
51000 Rijeka, Croatia
Phone: +385 (51) 770 447
Fax: +385 (51) 686 166
www.intechopen.com

InTech China

Unit 405, Office Block, Hotel Equatorial Shanghai
No.65, Yan An Road (West), Shanghai, 200040, China
中国上海市延安西路65号上海国际贵都大饭店办公楼405单元
Phone: +86-21-62489820
Fax: +86-21-62489821

© 2011 The Author(s). Licensee IntechOpen. This is an open access article distributed under the terms of the [Creative Commons Attribution 3.0 License](#), which permits unrestricted use, distribution, and reproduction in any medium, provided the original work is properly cited.

IntechOpen

IntechOpen